ChemComm

COMMUNICATION

View Article Online
View Journal | View Issue

Cite this: *Chem. Commun.*, 2025, **61**, 16428

Received 2nd June 2025,
Accepted 7th September 2025

DOI: 10.1039/d5cc03014e

rsc.li/chemcomm

A rapid covalent tracer to image aggresomes in stressed live cells

Mengdie Wang,[ab] Wang Wan,[ab] Jialu Sun[a] and Yu Liu *[ab]

The commercial PROTEOSTAT aggresome detection kit is not compatible with live-cell applications. Here, we report a rapid covalent fluorescent tracer to visualize aggresomes in stressed live cells without cell fixation.

Studying the well-defined 3-dimensional conformations of proteins is essential to understanding their proper physiological functions. The fidelity of protein folding is governed by the proteostasis network in cells, which regulates the integrity of the proteome from protein expression to degradation.[1] Proteostasis, however, tends to be disrupted by either endogenous or external stressors, leading to aberrant protein misfolding and aggregation. Proteome aggregation underlies the etiology of numerous protein conformational diseases, particularly neurodegenerative diseases. Intracellular proteome aggregations (*i.e.* aggresomes) and extracellular amyloid depositions (*i.e.* amyloid plaques) are common pathological hallmarks of these diseases.[2,3]

Much progress has been made in detecting protein aggregation using fluorescent sensors. Regarding extracellular amyloid deposition, amyloid proteins have been visualized by various types of sensors, including derivatives of BODIPYs,[4,5] curcumins,[6] aggregation-induced emission (AIE) probes,[7,8] metal coordination complexes,[9,10] and fluorescent protein fluorophores.[11] In the cellular milieu, the only commercially available system, the PROTEOSTAT aggresome detection kit, requires cell permeabilization and fixation before imaging aggresomes that consist of misassembled intracellular aggregated proteins.[12] Given the extent of cellular complexity, fluorescent tracers to detect aggresomes in live stressed cells are limited.[13–15] (Fig. 1a).

The abovementioned protein aggregation sensors are designed based on non-covalent binding mechanisms to sense the low-polarity and high-viscosity microenvironment inside protein aggregates. Alternatively, covalent tracers of a misfolded and aggregated proteome are developed by taking advantage of exposed and activated nucleophiles upon protein aggregation.[16] The Hong and Ohe groups developed fluorescent covalent tracers to label exposed thiol groups in response to unfolded proteins.[17–19] Though these covalent tracers of an unfolded proteome offer a stable fluorescence signal for imaging applications, covalent tracers for cellular aggresomes with rapid labelling kinetics have not yet been reported.

Herein, we introduced a Michael addition–based covalent fluorescent tracer to rapidly label and stably image cellular aggresomes in live stressed cells (Fig. 1b). The rapid covalent tracer may become useful for developing covalent proximity-inducing degradation drugs (ATTEC) to ameliorate proteome stress. We embarked on designing such a probe based on a fluorescent protein chromophore, a core scaffold reported to inherently bind to aggregated proteins (Fig. 2a).[13] To accelerate

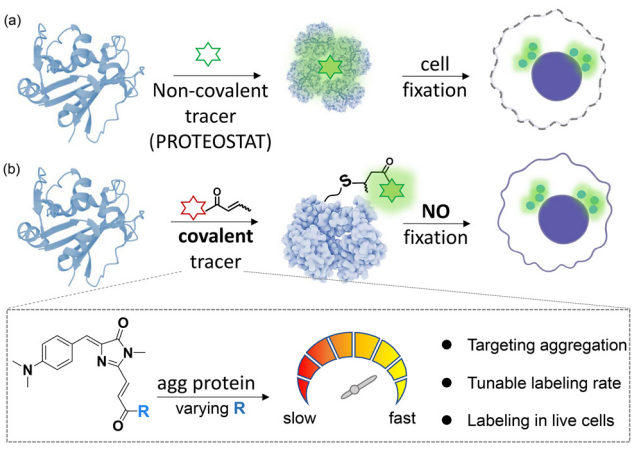

Fig. 1 Fluorescent tracers to detect cellular aggresomes in cells. (a) The non-covalent PROTEOSTAT kit requires cell fixation. (b) This work reported a rapid covalent chemical probe to track proteome aggregation in live cells *via* Michael addition with tunable labelling kinetics.

[a] *State Key Laboratory of Medical Proteomics, National Chromatographic R. & A. Center, Dalian Institute of Chemical Physics, Chinese Academy of Sciences, Dalian 116023, China. E-mail: liuyu@dicp.ac.cn*
[b] *University of Chinese Academy of Sciences, Beijing 100049, China*

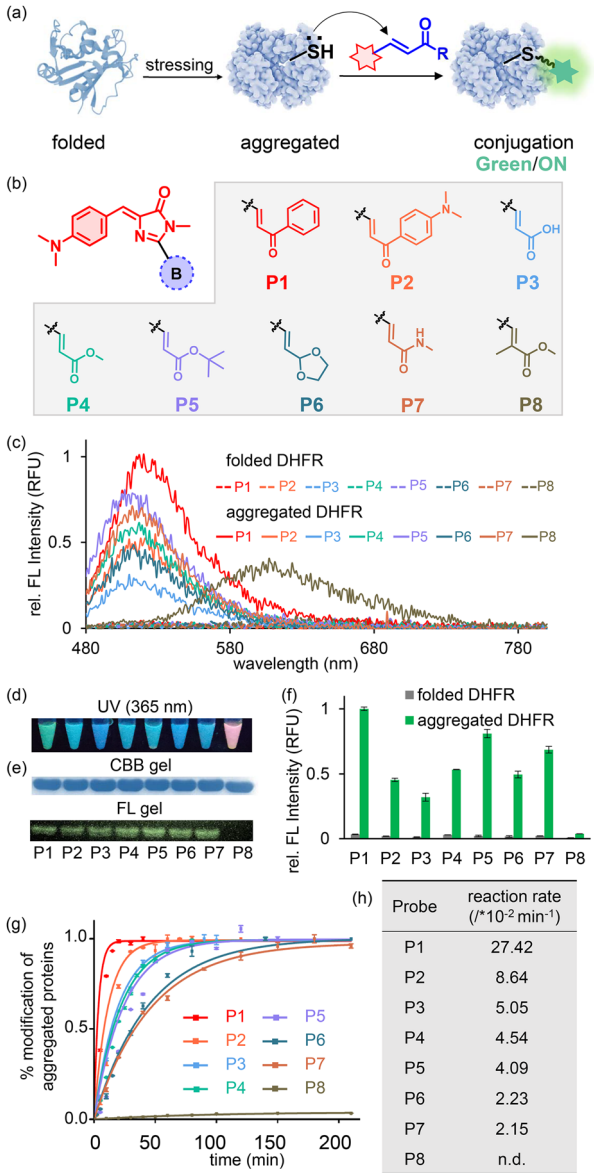

(h)

Probe	reaction rate (/*10^{-2} min^{-1})
P1	27.42
P2	8.64
P3	5.05
P4	4.54
P5	4.09
P6	2.23
P7	2.15
P8	n.d.

Fig. 2 Tuning the labelling kinetics of covalent protein aggregation sensors by modulating the reactivity of the Michael acceptor. (a) The mechanism of action to detect aggregated proteins with the fluorescent covalent sensor. (b) Structural modulation to regulate the reactivity of Michael acceptors. (c) The change in emission spectra of P1-P8 upon DHFR aggregation. (d) A photograph of aggregated DHFR incubated with P1–P8. P1–P7, but not P8, color-switched from red to cyan upon heat-induced DHFR aggregation. (e) Gel electrophoresis confirmed the covalent conjugation of probes with aggregated DHFR. (f) The relative maximum FL emission intensities of P1-P8 with aggregates. (g) The labelling kinetics of P1-P8 with aggregated DHFR. (h) Apparent labelling rates when fitted with pseudo-1st order kinetics.

the labelling kinetics, we rationally tuned the chemical reactivity of the Michael acceptor, resulting in probes P1 to P8 (Fig. 2b). As expected, all probes remained non-fluorescent with folded proteins (Fig. 2c: dashed lines) but fluorescence turned on upon binding and reacting with aggregated proteins (Fig. 2c: solid lines; Fig. S3). Notably, P8 with steric hindrance showed exclusively red fluorescence with an emission maximum at 605 nm, well aligned with the parent FP chromophore in viscous solvent (Fig. S7), indicating the negligible covalent reactivity of P8 towards aggregated proteins due to steric issues. In contrast, P1 to P7 all shifted their fluorescent emission from the red region to the cyan/green region (λ_{em} from 500 nm to 530 nm), suggesting that conjugation breaks upon Michael addition to aggregated proteins (Fig. 2c and d). It was noteworthy that extremely strong electron-withdrawing moieties may intensively quench fluorescence after conjugation (Fig. S9 and S10). The covalency upon conjugating to aggregated proteins was eventually evidenced *via* fluorescent SDS-PAGE gel (Fig. 2e).

Next, we asked whether these Michael acceptors with different electron densities can enhance the labelling kinetics, resulting in a rapid covalent tracer for protein aggregates. We took advantage of green fluorescence emission to monitor the covalent conjugation reaction between the probes and protein aggregates (Fig. 2f). To compare the reactivity of these probes toward protein aggregates, the labelling kinetics were quantified (WT-DHFR: 100 μM; probe: 10 μM; Fig. 2g). The apparent reaction rates for Michael addition were obtained by fitting with pseudo-first order kinetics, showing that chemical modulation *via* carbonyl substitution effectively tuned the labelling kinetics (Fig. 2h). Specifically, aryl ketones (P1–P2) were more rapid in labelling aggregated proteins compared to α,β-unsaturated carboxylic esters/acids (P3–P7). As expected, P8 with steric hindrance showed no covalent reactivity. Among all the probes, P1 offered the fastest labelling kinetics with a half-life ($t_{1/2}$) of 2.5 min. By tuning the structure of the Michael acceptor, we successfully accelerated the labelling kinetics from 0.036 s^{-1} for P7 up to 0.457 s^{-1} for P1. However, the fact that P1 with an electron-rich Michael acceptor offers the fastest labelling kinetics is contrary to our expectations; it may be because an additional benzene ring (P1 and P2) may contribute to better binding to aggregated proteins (*i.e.* faster k_{on}).

We further investigated the labelling mechanism of P1, the fastest probe shown in Fig. 2. First, we demonstrated that the green fluorescence was caused by protein aggregation. From fractionation experiments, the fluorescence signal was nearly all from the insoluble fraction, not from the soluble fraction. Analysis based on Coomassie bright blue (CBB), fluorescent gels and photographs under 365-nm UV light together echoed this conclusion (Fig. 3b). These results confirmed that P1 fully converted to green fluorescence upon conjugating to aggregated proteins. Next, we ensured that the labelling and consequent color-shifting from red to green were caused by conjugating to a nucleophile *via* nucleophilic 1,4-addition with P1. We selected protected cysteine and ethylamine to mimic cysteine and lysine nucleophilic residues, respectively, in aggregated proteins. The P1 probe effectively reacted with the model substrates, and the corresponding adducts were verified *via* high-resolution mass spectrometry (Fig. 3c). Similar to the scenario with protein aggregates (Fig. 2c), we observed hypsochromic shifts in both absorption and fluorescence emission (red to green) (Fig. 3d) in viscous glycerol, well aligned with that observed with protein aggregates. This observation indicated

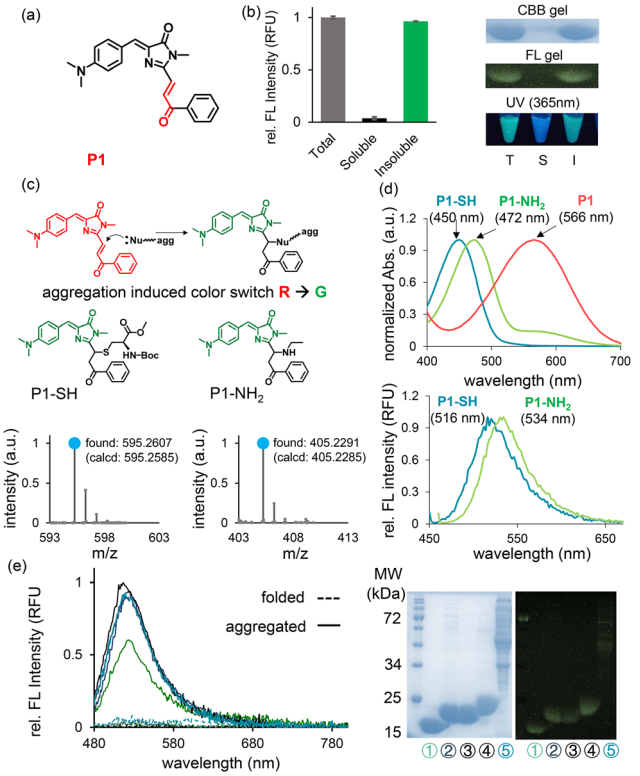

Fig. 3 P1 showed turned-on green fluorescence upon protein aggregation. (a) The structure of the P1 probe, the most rapid tracer for the covalent labelling of aggregated proteins. (b) Fractionation experiments indicating the fluorescence emission of P1 was mainly from conjugating to insoluble aggregates. T: total fraction, S: soluble fraction, I: insoluble fraction. (c) The color of P1 switched from red to green upon Michael addition with nucleophiles. High-resolution mass spectrometry verifying the expected Michael addition products. (d) UV-vis and fluorescence emission spectra from P1 after conjugating to nucleophilic cysteine and lysine. (e) The fluorescence emission spectra of P1 with folded and aggregated proteins and fluorescent gel electrophoresis, indicating that P1 is covalently conjugated to proteins.

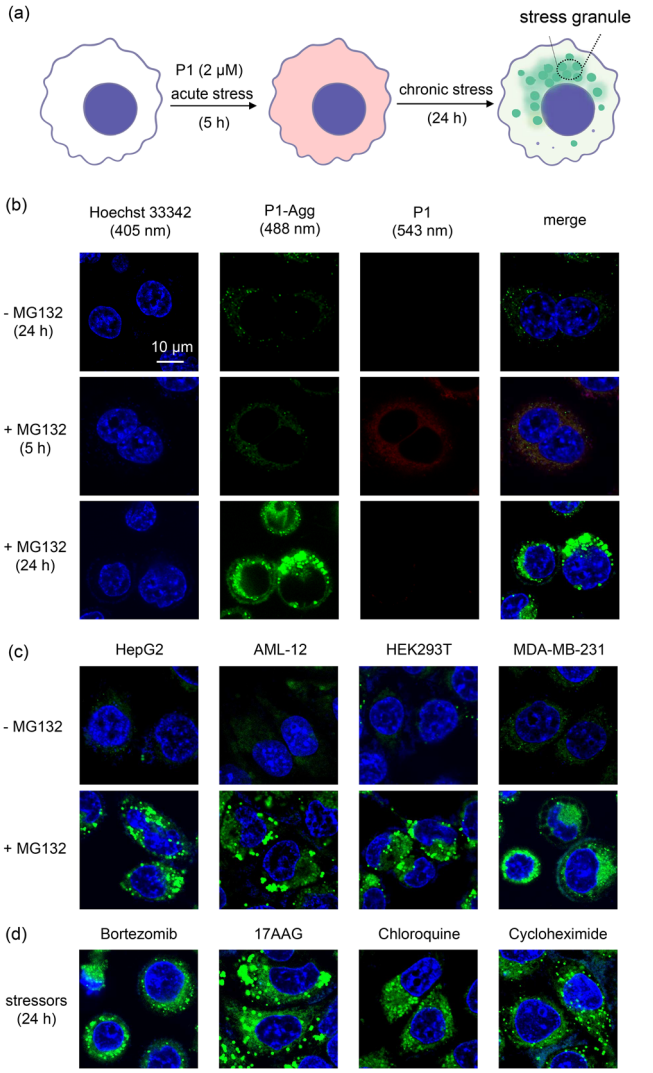

Fig. 4 Imaging cellular aggresomes with P1. (a) Experimental scheme for using P1 to label proteome aggregation in the cellular milieu without fixation. (b) Proteome aggregation induced by MG132 in HEK293T cells for different lengths of time: 5 h caused acute stress and initial proteome misfolding; 24 h caused prolonged stress and intense insoluble aggregates accumulated as aggresomes. P1 detected aggresomes in different cell lines (c) and in response to different cellular stressors (d).

that the fluorescence shift to a green color was indeed caused by Michael addition to nucleophiles inside aggregates. Moving forward to the aggregated protein scenario, P1 predominantly conjugated with the thiol groups of cysteine residues instead of other nucleophilic residues (Fig. S4).

We further validated the generality of the P1 probe for the covalent labelling of different types of aggregated proteins. Upon exposure to different aggregated recombinant proteins (50 μM) or lysate proteome (1 mg mL^{-1}), P1's green fluorescence gradually enhanced as the temperature increased after Michael addition to the protein aggregates (Fig. 3e). Fluorescence gel electrophoresis also confirmed the general covalent conjugation of P1 with these aggregates. Furthermore, we also used P1 to measure the thermodynamic stabilities of these proteins in thermal shift assays enabled by P1's green fluorescence (Figs S4 and S5).

Finally, we demonstrated that P1 served as a covalent tracer to selectively visualize aggresomes in stressed live cells without an unnecessary initial fixation protocol. According to the abovementioned fluorescence switching properties in buffer, P1 lit up with weak red fluorescence emission upon non-covalent binding with misfolded proteins in the initial acute stress phase but further switched to green color upon conjugating to insoluble aggregates accumulated in cellular aggresomes (Fig. 4a). To show these properties of P1, cellular proteome aggregation was induced by MG132 to inhibit proper proteosome function, leading to the formation of aggresomes. Upon short-term acute stress from MG132 for 5 h, a weak diffuse red fluorescence signal was observed in cytosol. Severe proteome aggregation in cells was observed after prolonged treatment with MG132 for 24 h. Meanwhile, punctate aggresome structures with intense green fluorescence were observed exclusively in the 488-nm channel (Fig. 4b). Such transformation of the

fluorescence color echoed the *in vitro* experimental results using recombinant proteins (Fig. 3).

To further demonstrate its general applicability, the P1 probe was also applied to detecting aggresomes in different cell lines, including liver cells (AML-12) from *Mus musculus*, and renal epithelial cells (HEK293T), hepatic cancer cells (HepG2), and breast cancer cells (MDA-MB-231) from *Homo sapiens*. As expected, P1 emitted bright green fluorescence upon labelling aggresomes after stressing the cells with MG132 for 24 h (Fig. 4c). In addition to MG132, other cellular stressors were also tested to demonstrate P1's general applicability for staining aggresomes, including 17AAG (heat-shock protein inhibitor), bortezomib (proteosome inhibitor), chloroquine (lysosome inhibitor) and cycloheximide (disturbs protein synthesis in ribosomes) (Fig. 4d). We observed different morphologies of cellular aggresomes under these stress conditions.

In summary, we developed a rapid covalent tracer to label aggregated proteins *via* Michael addition. The reaction rate was rationally tuned by chemical modifications, yielding up to 10-fold kinetic acceleration. The optimized probe P1 was used to monitor protein aggregation and rapidly label cellular aggresomes in multiple cell lines and under stress conditions. It is not always beneficial to improve the labeling kinetics by enhancing the electron-withdrawing capacity to the extreme while sacrificing selectivity. Balancing rapid labeling and satisfactory cellular selectivity is a challenge to be overcome by chemical fine-tuning. Our rapid covalent aggresome tracer outperformed the commercial PROTEOSTAT kit with better live-cell compatibility without fixation.

M. Wang: data curation, formal analysis, methodology, software, investigation, visualization. W. Wan: supervision, resources, validation, funding acquisition, writing – original draft. J. Sun: resources, validation. Y. Liu: conceptualization, funding acquisition, project administration, writing – review and editing.

This work was supported, in part, by funds from the National Natural Science Foundation of China (22222410, 22374148), Dalian Science and Technology Innovation Fund (2023JJ12WZ037), International Partnership Program of Chinese Academy of Sciences (028GJHZ2023079FN), and Innovation Program of Science and Research from the DICP, CAS (DICP I202458).

Conflicts of interest

There are no conflicts to declare.

Data availability

The data supporting this article have been included as part of the supplementary information (SI). Supplementary information: Supplementary figures, experimental procedures, synthesis and NMR spectra. See DOI: **https://doi.org/10.1039/d5cc03014e**.

Notes and references

1 M. S. Hipp, P. Kasturi and F. U. Hartl, *Nat. Rev. Mol. Cell Biol.*, 2019, **20**, 421–435.
2 W. E. Balch, R. I. Morimoto, A. Dillin and J. W. Kelly, *Science*, 2008, **319**, 916–919.
3 F. Chiti and C. M. Dobson, *Annu. Rev. Biochem.*, 2017, **86**, 27–68.
4 P. Verwilst, H. R. Kim, J. Seo, N. W. Sohn, S. Y. Cha, Y. Kim, S. Maeng, J. W. Shin, J. H. Kwak, C. Kang and J. S. Kim, *J. Am. Chem. Soc.*, 2017, **139**, 13393–13403.
5 B. Shen, K. H. Jung, S. Ye, C. A. Hoelzel, C. H. Wolstenholme, H. Huang, Y. Liu and X. Zhang, *Aggregate*, 2023, **4**, e301.
6 X. Zhang, Y. Tian, C. Zhang, X. Tian, A. W. Ross, R. D. Moir, H. Sun, R. E. Tanzi, A. Moore and C. Ran, *Proc. Natl. Acad. Sci. U. S. A.*, 2015, **112**, 9734–9739.
7 W. Fu, C. Yan, Z. Guo, J. Zhang, H. Zhang, H. Tian and W. H. Zhu, *J. Am. Chem. Soc.*, 2019, **141**, 3171–3177.
8 Y. Hong, L. Meng, S. Chen, C. W. Leung, L. T. Da, M. Faisal, D. A. Silva, J. Liu, J. W. Lam, X. Huang and B. Z. Tang, *J. Am. Chem. Soc.*, 2012, **134**, 1680–1689.
9 L. Ge and Y. Tian, *Anal. Chem.*, 2019, **91**, 3294–3301.
10 B. Jiang, A. Aliyan, N. P. Cook, A. Augustine, G. Bhak, R. Maldonado, A. D. S. McWilliams, E. M. Flores, N. Mendez, M. Shahnawaz, F. J. Godoy, J. Montenegro, I. Moreno-Gonzalez and A. A. Mart, *J. Am. Chem. Soc.*, 2019, **141**, 15605–15610.
11 H. Leng, Y. Wang, J. Wang, H. Sun, A. Sun, M. Pistolozzi, L. Zhang and J. Yan, *Anal. Chem.*, 2022, **94**, 1999–2006.
12 S. Navarro and S. Ventura, *Biotechnol. J.*, 2014, **9**, 1259–1266.
13 W. Wan, W. Jin, Y. Huang, Q. Xia, Y. Bai, H. Lyu, D. Liu, X. Dong, W. Li and Y. Liu, *Anal. Chem.*, 2021, **93**, 1717–1724.
14 Y. Huang, M. Chang, X. Gao, J. Fang, W. Ding, J. Liu, B. Shen and X. Zhang, *ACS Cent. Sci.*, 2024, **10**, 842–851.
15 B. Shen, L. Liu, Y. Huang, J. Wu, H. Feng, Y. Liu, H. Huang and X. Zhang, *Aggregate*, 2024, **5**, e421.
16 W. Wan, Y. Huang, Q. Xia, Y. Bai, Y. Chen, W. Jin, M. Wang, D. Shen, H. Lyu, Y. Tang, X. Dong, Z. Gao, Q. Zhao, L. Zhang and Y. Liu, *Angew. Chem., Int. Ed.*, 2021, **60**, 11335–11343.
17 H. Mu, K. Miki, T. Kubo, K. Otsuka and K. Ohe, *Chem. Commun.*, 2021, **57**, 1818–1821.
18 T. C. Owyong, P. Subedi, J. Deng, E. Hinde, J. J. Paxman, J. M. White, W. Chen, B. Heras, W. W. H. Wong and Y. Hong, *Angew. Chem., Int. Ed.*, 2020, **59**, 10129–10135.
19 S. Sabouri, M. Liu, S. Zhang, B. Yao, H. Soleimaninejad, A. A. Baxter, G. Armendariz-Vidales, P. Subedi, C. Duan, X. Lou, C. F. Hogan, B. Heras, I. K. H. Poon and Y. Hong, *Adv. Healthcare Mater.*, 2021, **10**, e2101300.